12-1-2020

Modeling an auditory stimulated brain under altered states of consciousness using the generalized ising model

Sivayini Kandeepan
The University of Western Ontario

Jorge Rudas
Universidad Nacional de Colombia

Francisco Gomez
Universidad Nacional de Colombia

Bobby Stojanoski
The University of Western Ontario

Sreeram Valluri
The University of Western Ontario

See next page for additional authors

NeuroImage 223 (2020) 117367

Contents lists available at ScienceDirect

NeuroImage

journal homepage: www.elsevier.com/locate/neuroimage

Modeling an auditory stimulated brain under altered states of consciousness using the generalized ising model

Sivayini Kandeepan[a,b,*], Jorge Rudas[c], Francisco Gomez[c], Bobby Stojanoski[d], Sreeram Valluri[a], Adrian Mark Owen[d], Lorina Naci[e], Emily Sophia Nichols[d,#], Andrea Soddu[a,#]

[a] Department of Physics and Astronomy and the Brain and Mind Institute, University of Western Ontario, 1151 Richmond St, London, ON, N6A 3K7, Canada
[b] Department of Physics, Faculty of Applied Sciences, University of Sri Jayewardenepura, Nugegoda, Sri Lanka
[c] Department of Mathematics, Universidad Nacional de Colombia, Cra 45, Bogotá, Colombia
[d] Brain and Mind Institute, University of Western Ontario, 1151 Richmond St, London, Ontario, N6A 3K7, Canada
[e] Trinity College Institute of Neuroscience, Trinity College Dublin, College Green, Dublin 2, Ireland

ARTICLE INFO

Key words:
The generalized ising model
Naturalistic stimuli
Inter-subject correlation
Consciousness

ABSTRACT

Propofol is a short-acting medication that results in decreased levels of consciousness and is used for general anesthesia. Although it is the most commonly used anesthetic in the world, much remains unknown about the mechanisms by which it induces a loss of consciousness. Characterizing anesthesia-induced alterations to brain network activity might provide a powerful framework for understanding the neural mechanisms of unconsciousness.

The aim of this work was to model brain activity in healthy brains during various stages of consciousness, as induced by propofol, in the auditory paradigm. We used the generalized Ising model (GIM) to fit the empirical fMRI data of healthy subjects while they listened to an audio clip from a movie. The external stimulus (audio clip) is believed to be at least partially driving a synchronization process of the brain activity and provides a similar conscious experience in different subjects. In order to observe the common synchronization among the subjects, a novel technique called the inter subject correlation (ISC) was implemented.

We showed that the GIM—modified to incorporate the naturalistic external field—was able to fit the empirical task fMRI data in the awake state, in mild sedation, in deep sedation, and in recovery, at a temperature T^* which is well above the critical temperature. To our knowledge this is the first study that captures human brain activity in response to real-life external stimuli at different levels of conscious awareness using mathematical modeling. This study might be helpful in future to assess the level of consciousness of patients with disorders of consciousness and help in regaining their consciousness.

1. Introduction

The brain is a complex system, characterized by heterogeneous networks of structural connections supporting cognition, and which assist in responding to perceptual information coming from the peripheral nervous system. Modern neuroimaging techniques, such as fMRI and EEG, now permit the comprehensive mapping of these networks in order to understand how information is transmitted within and across them (Abreu et al., 2018). However, many aspects of the dynamical functioning of the brain under stimulation and in altered states of consciousness induced by anesthetic drugs are still not completely understood (Hudetz, 2012). Using engaging stimuli that drive a specific conscious experience (such as, for example, watching a movie) would make it possible to detect whether behaviourally unresponsive patients are having a comparable conscious experience.

Anesthetics generally suppress the body's normal automatic functions, such as breathing, the heartbeat, and blood pressure, as well as the global cerebral metabolic rate (Will and Berg, 2007). Using EEG, it has been shown that low-frequency, high amplitude oscillations increase as the level of anesthesia increases (Hagihira, 2015). A number of neuroimaging studies have probed the effects of anesthesia-induced sedation on brain activation when exposed to various types of acoustic inputs. Using propofol, a short-acting medication that results in a decreased level of consciousness that is widely used due to its fast in-

* Corresponding author: Sivayini Kandeepan. Department of Physics and Astronomy, University of Western Ontario, 1151 Richmond St, London, Ontario, N6A 3K7, Canada.
E-mail addresses: skandee@uwo.ca, ssivayini@sjp.ac.lk (S. Kandeepan).
# Authors contributed equally

https://doi.org/10.1016/j.neuroimage.2020.117367
Received 2 February 2020; Received in revised form 8 August 2020; Accepted 8 September 2020
Available online 12 September 2020

duction and recovery time (Tobias and Leder, 2011), Naci et al. found a high cross-subject correlation between sensory-driven auditory cortex in higher-order frontal and parietal regions while listening to a plot-driven audio story while participants were conscious. During deep anesthesia, however, the cross-subject correlation was limited to the auditory cortex, and was almost abolished in fronto-parietal regions (Naci et al., 2014). Davis and colleagues also found that bilateral temporal-lobe responses to complex auditorily-presented sentences were preserved when reduced levels of awareness were induced via propofol (Davis et al., 2007). These findings were further confirmed by Dueck et al., who presented musical stimuli to neurosurgical patients after the injection of different concentrations of propofol (Dueck et al., 2005). Their study showed activation in the superior temporal gyrus (primary and secondary auditory cortex) and in higher-order auditory information processing areas while participants were awake. These activations attenuated with increasing concentrations of propofol but remained partially preserved in the superior temporal gyrus. Additionally, in an auditory word listening fMRI study of functional connectivity, Liu et al. reported that propofol-induced sedation disrupted verbal comprehension and memory by blocking the projection of sensory information to higher-order processing networks and thus preventing information integration (Liu et al., 2012).

Neuroimaging techniques have allowed us to explore how the brain functions at different levels of consciousness, in both healthy individuals and in patients. However, there are many hypotheses that would be difficult or impossible to directly test using brain imaging. Computational models allow us to simulate the brain in different states and under different conditions, allowing us to test such hypotheses. One such model, the Ising model developed by Ernest Ising, has been adapted from its traditional use in describing the behaviour of magnets to be applied in computational neuroscience (Fraiman et al., 2009; Schaub and Schultz, 2012). Spin sites capture the dynamics of the BOLD signal with a two-state spin variable, representing activity above and below a baseline. By simulating the Ising model at different temperatures, Fraiman et al. showed that, at the critical temperature *Tc* (the temperature at which the system exhibits a transition from an ordered phase to a disordered phase), the model can simulate the global behavior of the brain's functional connectivity at rest (Fraiman et al., 2009). They showed that the best fit to the distribution of the functional correlations of the brain was obtained from the simulations at the critical temperature of the 2D classical Ising model.

The generalized Ising model (GIM), which was introduced by Marinazzo and colleagues (Marinazzo et al., 2014), is a modification to the 2D classical Ising model, in which spins are no longer restricted to interact with only their neighbours, but may interact with all other spins via differing coupling strengths (Marinazzo et al., 2014). In the classical Ising model, spins of the lattice do not correspond to a particular region of the brain, however in the generalization of the Ising model, each brain region corresponds to a particular spin in the lattice site. Accordingly, the structural connectivity matrix *Jij*, which gives the coupling strength between two regions in the model, is built such that it corresponds to the number of white matter fibers between each pair of regions of the brain obtained using diffusion tensor imaging (DTI). Because we have parcellated the brain into 84 regions, *Jij* is an 84×84 matrix and the couplings are normalized in such a way that the highest coupling has a value of one. Considering this one-to-one relationship between the spin sites and the brain regions, this model can be used to simulate the BOLD activity either during resting state (spontaneous activity) or while engaged in a task.

The GIM has been recently employed to simulate resting state fMRI (Abeyasinghe et al., 2018; Das et al., 2014; Deco et al., 2012; Fraiman et al., 2009; Marinazzo et al., 2014; Stramaglia et al., 2017). Implementing the GIM on two different resolutions of structural connectivity matrices, Marinazzo et al. showed that the total information transfer between the spins, defined by the Shannon entropy, was maximized at criticality (Marinazzo et al., 2014). Further, Stramaglia and colleagues compared the correlations between spin sites simulated from the Ising model implemented on the structural connectome against the empirical functional brain correlations both at the single link level (in which spin sites are flipped one at a time) and at the modular level (in which blocks of correlated spin sites are flipped together). They concluded that when the brain is under anesthesia, similarity between the model and empirical data increases at the modular level (Stramaglia et al., 2017).

Continuing work to optimize the GIM, Deco et al. studied the Ising model implemented on artificially created structural connectomes with different coupling strengths among the nodes (Deco et al., 2012). By examining the entropy of the system at different coupling strengths, they found that the system exhibited rich dynamics when the structural connections of the brain self-organized to form a scale-free network. Such a network is characterized by many nodes with high connections (i.e., hubs), following a power-law degree distribution. They are called scale-free, as power laws have same functional form at any scale. Finally, Abeyasinghe et al. (Abeyasinghe et al., 2018) calculated the dimensionality of the brain with respect to information transfer during wakefulness, using the GIM, and reported it to be two. In their work, dimensionality was explained in terms of the reactivity of neurons to stimuli, that is, neurons specialized to react to certain stimuli were low dimensional, while neurons that react to mixed stimuli were highly dimensional. In order to calculate dimensionality, they introduced a concept for the distance between two regions in the GIM to be equivalent to the inverse of the normalized fiber connections between the two regions (which is relevant to the information transfer), as there is no direct measure to calculate the distance between the two regions in the GIM.

The goal of the present study was to provide an initial step to see if the GIM can be applied to assess the common neural experience a behaviourally non responsive patient might have. To do this, we modelled the brain activity of healthy subjects using the GIM implemented on the structural architecture, in altered states of consciousness, while receiving a naturalistic external stimulus. We predicted that the brain-behaviour response to naturalistic stimuli would be more complex to model compared to stimuli presented in a block design. This study in future might provide an alternative way to measure the awareness of a non-responsive patient and help in restoring their consciousness.

2. Methodology

The data of 17 healthy subjects were acquired while participants were listening to the audio clip (task condition) as well as while they were at rest, at four levels of sedation. Data were then preprocessed and parcellated into 84 regions of interest (ROIs), and the empirical time series of each ROI was extracted. The GIM was then simulated at different temperatures under resting and task conditions, and simulated time series were obtained. Empirical and simulated inter-subject correlations were calculated using the respective time series, and they were then compared to find the temperature that led to the highest degree of similarity. Details of each step are given below.

2.1. Participants

17 healthy volunteers (4 women; mean age 24 years, SD = 5) participated in this study. All were right-handed, native English speakers, and had no history of neurological disorders, and were recruited via printed advertisements posted on the university campus and through word of mouth. All volunteers provided informed consent after completing an MRI and propofol safety screening questionnaire provided by both the attending MR technician and anesthesiologist, to confirm that they understood study risks and did not have any contraindications for MRI or sedation. Volunteers were remunerated for their time. Ethical approval was obtained from the Health Sciences Research Ethics Board and Psychology Research Ethics Board of Western University (REB #104,755).

2.2. Task Protocol

FMRI scans were acquired while participants listened to the audio story in four states of consciousness: awake, mild sedation, deep sedation, and recovery. The audio story was played at the start of each session once the wakefulness/sedation level was assessed. The audio story was 5 min in duration and was an excerpt from a scene of the movie 'Taken' (reported in Naci et al., 2015) that portrays a teenage girl being kidnapped (Naci et al., 2017). This audio story was chosen because it is richly evocative and highly arousing as well. The study was approved by the ethics committee of the Health Sciences Research Ethics Board and Psychology Research Ethics Board of the University of Western Ontario. Written informed consent to participate in the study was obtained from the subjects. The data used in this study will be available in Openneuro.org.

2.3. Administration of propofol

Before entering the fMRI scanner, a 20 G i.v. cannula was inserted into a vein on the dorsum of the non-dominant hand of the participants. The propofol infusion system was connected to the cannula prior to the first scanning session. Intravenous propofol was administered with a Baxter AS 50 (Singapore). An effect-site/plasma steering algorithm was used in combination with the computer-controlled infusion pump to achieve step-wise increments in the sedative effect of propofol. The infusion pump was adjusted to achieve the desired level of sedation, guided by targeted concentrations of propofol, as predicted by the TIVATrainer (the European Society for Intravenous Aneaesthesia, eurosiva.eu) pharmacokinetic simulation program. The pharmacokinetic model provided target-controlled infusion by adjusting infusion rates of propofol over time to achieve and maintain the target blood concentrations as specified by the Marsh 3 (Marsh et al., 1991) compartment algorithm for each participant, as incorporated in the TIVATrainer software.

The four states of consciousness were defined as follows. **1) Awake**: No propofol was administered during the "awake" session. During the awake scan, prior to the administration of propofol, participants were fully awake, alert, and communicating appropriately. **2) Mild sedation**: At the beginning of the mild sedation scan, propofol infusion commenced with a target effect-site concentration of 0.6 μg/ml and oxygen was titrated to maintain SpO_2 above 96%. Once the baseline target effect-site concentration was reached, the participants' level of sedation was assessed and if deemed to be appropriate for mild sedation (Ramsey 3), the effect-site concentration was maintained. During administration of propofol, participants became calmer and more slowed in their response to verbal communication. Once participants stopped engaging in spontaneous conversation, and speech became sluggish, they were classified as a Ramsey level 3 and were considered mildly sedated. At this level, participants only responded to loud commands. **3) Deep sedation**: Prior to commencing the deep sedation scan, the target effect-site concentration was again increased in increments of 0.3 μg/ml with repeated assessments of responsiveness. Once a Ramsey 5 level of sedation was achieved, no further changes were made, and the participant was maintained at that level. When participants stopped responding to verbal commands and were only rousable to light physical stimulation, they were considered Ramsey level 5 and deeply sedated. Patients were unable to engage in conversation at this level. At Ramsay 5, participants remained capable of spontaneous cardiovascular function and ventilation. **4) Recovery**: Propofol was discontinued following the deep sedation scan and approximately 11 min following the discontinuation of propofol, participants reached Ramsey level 2. This was observed by clear and quick responses to verbal commands.

The mean estimated effect-site propofol concentration was 2.48 (1.82–3.14) μg/ml, and the mean estimated plasma propofol concentration was 2.68 (1.92–3.44) μg/ml. Mean total mass of propofol administered was 486.58 (373.30–599.86) mg. The variability of these concentrations and doses is typical for studies of the pharmacokinetics and pharmacodynamics of propofol (Nimmo et al., 2019; Sukumar et al., 2018).

2.4. Sedation Assessment

Prior to acquiring fMRI data, three independent assessors (two anesthesiologists and one anesthesia nurse) evaluated each participant's Ramsay level by communicating with them in person inside the fMRI scanner room. Participants were also asked to perform a basic verbal recall memory test and a computerized (4 min) auditory target detection task, which further assessed each individual's wakefulness/sedation level independently of the anesthesia team. Scanning commenced only when the agreement among the three anesthesia assessors on the wakefulness/sedation level was confirmed.

2.5. fMRI Data acquisition

Noise cancellation headphones (Sensimetrics, S14; www.sens.com) were used for sound delivery at a volume level deemed comfortable by each individual for the duration of the experiment. Functional echo-planar images were acquired (33 slices, voxel size: $3 \times 3 \times 3$ mm^3, inter-slice gap of 25%, TR = 2000 ms, TE = 30 ms, matrix size = 64×64, FA = 75°). The audio story and resting state scans had 155 and 256 vol, respectively. An anatomical scan was obtained using a T1-weighted 3D MPRAGE (Magnetization Prepared - RApid Gradient Echo) sequence (32 channel coil, voxel size: $1 \times 1 \times 1$ mm^3, TE = 4.25 ms, matrix size = $240 \times 256 \times 192$, FA = 9°).

2.6. Preprocessing of fMRI data

T1 images were preprocessed using the SPM (http:www.fil.ion.ucl.ac.uk/spm), FSL (https://fsl.fmrib.ox.ac.uk/fsl/fslwiki/), SimpleITK (http://www.simpleitk.org/) and Dipy (http://nipy.org/dipy/) toolboxes. T1 preprocessing included manual removal of the neck, brain extraction using FSL, correction of low-frequency intensity non-uniformity based on the N4 (non-parametric non-uniform normalization) bias field correction algorithm from SimpleITK, image denoising based on non-local means algorithm from Dipy, and spatial normalization to standard stereotactic Montreal Neurological Institute (MNI) space using the SPM12 normalization algorithm. The initial three volumes of the fMRI data were discarded to avoid T1 saturation effects. Head motion and slice timing corrections were performed on the fMRI data using FSL, followed by artifact correction using RapidArt (https://www.nitrc.org/projects/rapidart/). Subsequently, fMRI data were coregistered to a T1 image using SPM12 (http:www.fil.ion.ucl.ac.uk/spm) and spatially normalized to MNI space using the SPM12 normalization algorithm. Finally, spatial smoothing of the fMRI data was performed with a Gaussian kernel of 8 mm full-width at half maximum as implemented in SPM12.

2.7. fMRI Signal extraction based on parcellation

First, the average time series of each region inside the AAL2 parcellation (Hagmann et al., 2008) scheme (http://www.gin.cnrs.fr/en/tools/aal-aal2/) was extracted. The extracted time series were then cleaned by removing spurious variance via the regression of nuisance waveforms derived from the average time series obtained from regions of non-interest (white matter and cerebrospinal fluid). This nuisance regressor also included six motion parameters (translation and rotation parameters in the x, y, and z dimensions) from a rigid body transformation previously estimated using FSL. Finally, the time series were detrended, filtered using a bandpass with a Butterworth filter of cut-off frequencies set at 0.01 Hz and 0.1 Hz, and standardized to have zero mean and unit variance across time.

2.8. Extraction of features from the audio clip

The spins of the GIM were coupled with the external field (i.e., the audio clip) via different coupling strengths. The coupling strengths were obtained by performing a general linear model (GLM) between the audio clip and the time series, using the audio clip as the independent variable and the time series of each region as the dependent variables. The coefficients calculated from the GLM represented the coupling strengths of each spin with the external field. Using the combination of the coupling strengths and the audio clip as the external stimulus, the GIM was simulated. However, the inter-subject correlation (will be discussed in Section 2.9) calculated from the simulated data was not able to fit the inter-subject correlation calculated from the empirical data at any temperatures. Therefore, more meaningful time and frequency domain features were extracted from the audio clip to simulate the GIM as follows.

The audio clip was sampled at 44.1 kHz for a duration of 5 min. Twenty-one audio features from both the time and frequency domains were extracted from the original audio clip using the software pyAudioAnalysis (https://github.com/tyiannak/pyAudioAnalysis/) (Giannakopoulos, 2015). In this extraction we only considered the audio features relevant in describing an engaging scene of a movie. Therefore, we did not extract other features which describe the melodic characteristics of music such as the chroma vector or chroma deviation, obtained from this pyAudioAnalysis software. The three time-domain features were: zero crossing rate (rate of sign changes along a signal), energy (sum of squares of the signal values, normalized by the respective frame length) and entropy of energy (measure of abrupt changes), which were directly extracted from the raw signal samples. The eighteen remaining features were in the frequency domain, obtained from the Fourier transform of the audio signal, and consisted of spectral centroid (center of gravity of the spectrum), spectral spread (second central moment of the spectrum), spectral entropy (entropy of the normalized spectral energies for a set of sub-frames), spectral flux (the squared difference between the normalized magnitudes of the spectra of the two successive frames), spectral roll off (the frequency below which 90% of the magnitude distribution of the spectrum is concentrated) and thirteen Mel frequency cepstral coefficients (MFCCs). MFCCs are coefficients that collectively make up a Mel frequency spectrum and offer a description of the spectral shape of the sound (Giannakopoulos, 2015). Here, the frequency bands are positioned logarithmically (on the Mel scale), which more closely approximates the human auditory system's perceived response or pitch than do the linearly-spaced frequency bands. The audio signal was divided into time frames with lengths of two seconds without overlap, to match the repetition time of the fMRI data, and the above-mentioned audio features were extracted using the average of each frame. Finally, a multicollinearity test was performed on these 21 extracted features after they were normalized between −1 and 1, using a function called "*variation inflation factor*" implemented in RStudio. This function determined that three features had higher collinearity and could therefore be removed, while the remaining 18 features were used in the generalized linear modelling.

2.9. Inter-Subject Correlation

Inter-Subject Correlation (ISC) has been used previously to examine highly complex fMRI data acquired during naturalistic stimulation, such as when watching a movie (Hasson et al., 2004; Kauppi et al., 2010; Pajula et al., 2012). ISC measures the common neural activity present across subjects by comparing their neural response time series over the course of the naturalistic stimulation. The main advantage of ISC analysis over conventional fMRI analysis is that it does not require *a priori* knowledge of the external stimulus to locate activated brain areas. In ISC analysis, the subject's brain response to naturalistic stimuli is used to predict the brain responses within other subjects. Therefore, it is a model-free approach and is useful in measuring the synchronization across brains, induced by the real-life stimulus.

Here, in order to calculate the ISC of the empirical data, the time series from each ROI was initially extracted from the preprocessed fMRI data using the method described in Sections 2.6 and 2.7, and normalized such that the highest value was ±1. Pearson correlations between every pair of subjects were calculated for each ROI using the formulae given in Eq. (1) and then averaged ($\bar{r}$) over the number of pairs using Eq. (2).

$$r_{ij} = \frac{\sum_{n=1}^{N}\left[\left(S_i[n]-\overline{S_i}\right)\left(S_j[n]-\overline{S_j}\right)\right]}{\sqrt{\sum_{n=1}^{N}\left(S_i[n]-\overline{S_i}\right)^2\sum_{n=1}^{N}\left(S_j[n]-\overline{S_j}\right)^2}} \tag{1}$$

$$\bar{r} = \frac{1}{\left(\frac{m^2-m}{2}\right)}\sum_{i=1}^{m}\sum_{j=2,j>i}^{m} r_{ij} \tag{2}$$

where r_{ij} is the correlation coefficient between the time series of the i^{th} and j^{th} subjects, N is the total number of samples in the time series, S_i and S_j are the time series obtained from i^{th} and j^{th} subjects, respectively, $\overline{S_i}$and $\overline{S_j}$ denote the means of S_i and S_j and m is the total number of subjects (in our case, $m = 17$). Then, in order to test for the statistical significance of $\bar{r}$, null re-sampling distribution was generated by circularly shifting the time series of each subjects by a random number. Then the re-sampled r_{ij} values were calculated. Afterwards, a t-test between the distributions of the original r_{ij} values and the re-sampled r_{ij} values of each ROI was performed. Results of the t-tests were Bonferroni corrected for multiple comparisons (McDonald, 2009) with a significance level of $p < 0.01$ to acquire only the significant $\bar{r}$-values. The ISC of the resting and task data was calculated for all four levels of consciousness, and plotted on a brain map using MATLAB.

2.10. Generalized Linear modelling

Generalized Linear Modelling (GLM) coefficients were used as an input to simulate the GIM. GLM was performed using the 18 audio features ($P(t)$) that survived the multicollinearity test as the independent variables, and the empirical time series as the dependent variable to obtain the coefficients. The coefficients represent the coupling of the external stimulus with the spin sites and we refer to the collective coefficients (84 in our case) of all the ROIs as the β-map. The GLM was repeated on all subjects' empirical data to obtain their β-maps for each audio features. A one-sample t-test was then performed on the audio features using the subjects' β-maps to obtain the t-scalar maps for each audio features. Only those t-values possessing a $p < 0.01$ were used to generate the external stimulus to be used in the GIM. The external stimulus for each condition (awake, mild sedation, deep sedation, recovery) was calculated via Eq. (3):

$$H_i(t) = \sum_{k=0}^{Np} P^k(t) t_i^k \tag{3}$$

where $H_i(t)$ is the external stimulus applied onto i^{th} region, Np is the total number of predictors (=18 in our case), t_i^k is the threshold t-value of the region i for the k^{th} predictor, obtained from the t-test among the β-values, $P^k(t)$ is the time series of the k^{th} predictor and $P^0 = 1$. This $H_i(t)$ was then used as the external stimulus while simulating the GIM.

2.11. Generalized Ising model simulation

The GIM used an initial 1-D random spin configuration with 84 spins in either the +1 or −1 state, and was in contact with a thermal bath of temperature T. The energy of the spin configuration during spontaneous activity (resting) and non-spontaneous activity (with external stimulus) are given by Eqs. (4) and (5), respectively:

$$E_{rest} = -\sum_{i,j;i\neq j}^{N} J_{ij} s_i s_j \tag{4}$$

$$E_{stim} = -\sum_{i,j;i\neq j}^{N} J_{ij} s_i s_j - \sum_{i}^{N} H_i(t) s_i \tag{5}$$

where J_{ij} is the coupling constant between the i^{th} and the j^{th} site (i.e., the number of fibers connecting two regions, normalized between 0 and 1), S_i and S_j are the spins of the i^{th} and j^{th} site, and N (=84) is the total number of spin sites. The J_{ij} was obtained from the averaged DTI data of 69 subjects from the Human Connectome Project. The Metropolis Monte Carlo (MMC) algorithm was employed to simulate the system. In order to minimize the energy of the spin configuration using the MMC algorithm, the following steps were performed: 1. A random initial configuration with 84 spins was generated and the initial energy (E_{in}) was calculated. 2. A randomly selected spin was flipped, and the new energy (E_{new}) was calculated. 3. If $E_{new} < E_{in,}$ the spin flip was accepted, the new configuration became the new initial configuration with energy $E_{in} = E_{new}$, and the simulation was continued from step 2. 4. If $E_{new} > E_{in,}$ the Boltzmann factor $B = exp^{-\frac{\Delta E}{k_B T}}$ was calculated and a random number r between 0 and 1 was drawn. If $B > r$, the spin was accepted, E_{in} was replaced with E_{new}, and the procedure was repeated from step 2. Alternatively, if $B < r$, the flip was rejected, and the simulation was started over from step 2. These simulations were repeated from step 2 until an equilibrium condition with minimal fluctuations around the equilibrium energy was reached. Once the system was allowed to equilibrate, the equilibrium energy (E), magnetization (M) and susceptibility (χ) were calculated using Eqs. (4)–(7):

$$M = \frac{1}{N}\left|\sum_{i=1}^{N} S_i\right| \tag{6}$$

$$\chi = \frac{1}{NT}\left[M^2 - M^2\right] \tag{7}$$

Simulation for one time-point in the GIM was considered equivalent after N x N x 10 (where N is the number of spins) number of flips had been performed. Previous work has empirically shown that with this number of steps, equilibrium will be reached and therefore the thermodynamic properties can be calculated (Abeysinghe et al., 2018; Fraiman et al., 2009). The time taken to perform this number of spin flips was considered to be equivalent to 2 s (one time-point) of the audio clip, as TR = 2 s. By repeating these steps to equal number of time points of fMRI data, each time confirming the equilibrium condition, the simulated time series were obtained.

The GIM was simulated for the resting ($H(t) = 0$) and task conditions ($H(t) \neq 0$) using the external stimulus $H(t)$ described in Section 2.10. This procedure was repeated for 250 different temperatures ranging from 0.025 to 6 (unit-less), and at each temperature, the thermodynamic properties such as the energy, magnetization and susceptibility were calculated. The simulations were performed 17 times, using different initial configurations to resemble 17 subjects, for all four levels of consciousness. Next, assuming that the temperature across the subjects was identical, the ISC was calculated on the generated time series for each of the 250 temperatures. The ISC maps calculated from the simulated time series were then plotted at the critical temperature (the temperature that maximized susceptibility), and the temperature that minimized the distance between the empirical and simulated ISC (i.e., the temperature that gave the best fit between the empirical and simulated ISC) which was calculated using Kolmogrove-Smirnov test (KS-test) statistic. The temperature at which this happens was considered as our best fit between the empirical and simulated ISC.

The null distribution for the ISC was generated in two ways; 1) by randomly permuting the J_{ij} and simulating the GIM using the same coupling terms 2) by randomly permuting the coupling terms and simulating the GIM using the un-permuted j_{ij}. Then, to look at the effects in the ISC due to the alterations in both j_{ij} and coupling terms, Pearson correlation coefficients between the empirical ISC and simulated ISC at T^* were obtained.

3. Results

Fig. 1 shows the ISC obtained from the empirical data for all four levels of consciousness, while the subjects were listening to the audio clip. Overall, a clear pattern of synchronization, which decreased with levels of unconsciousness and increased during the recovery stage was seen, consistent with what has been found previously (Boveroux et al., 2010; Jordan et al., 2013). In the awake condition, synchronization amongst participants' brain activity in the fronto-parietal, auditory, and language areas was observed. Synchronization amongst participants in the frontal-parietal area diminished in the mild and deep sedation conditions, but returned back to its original level during recovery. However, synchronization in the auditory regions remained during unconsciousness, with lower values, similar to results found in prior studies (Naci et al., 2018). In contrast, synchronization amongst participants' brain regions was not observed at any levels of consciousness during the resting conditions (i.e., when not listening to the audio clip).

Results obtained from the GIM simulations using the empirical data are presented in the following sections. Fig. 2 displays the variation of the thermodynamic properties during rest and under stimulation for sedated and non-sedated conditions. Plotted values are the mean of 17 simulations along with their standard deviations. The standard deviation at rest is very small and cannot be seen in the plots.

Critical temperatures in each condition were obtained using the maximum of the susceptibility curves shown in Fig. 2 and are plotted in Fig. 3. Overall, the critical temperature during stimulation shifted towards lower temperature values compared to the resting condition. During stimulation, the critical temperatures increased from awake to mild sedation, and further increased from mild to deep sedation; it then decreased during recovery and reached similar critical value as that of the awake state. However, during all four levels of consciousness, the critical temperature at rest remained the same at a value of 1.41. At rest, Tc did not change, as it depended only upon the input J_{ij}. In contrast, under stimulation, while we used the same Jij for all levels of consciousness we derived different t-maps to model the modulation of the anaesthetic on the different brain regions' interaction with the external field. Because Tc depends on both the structural connectivity (Jij) and the interaction of the spins with the external field, a change in Tc was observed for different levels of consciousness.

Fig. 4 depicts the distance between the normalized empirical and simulated ISC for the task data, calculated using the KS-test. The sub criticality ($T < Tc$), super criticality ($T > Tc$), and T_{min} (the temperature that minimizes the distance between the correlation matrices of empirical and simulated data) values are defined as published in Abeysinghe et al. (Abeysinghe et al., 2018). The criticality (Tc) is far lower than T^*, the temperature that minimizes the distance between the empirical and simulated ISC. From the results, we can conclude that in order to reach T^*, the system should be in a super critical state.

Normalized eighteen audio features extracted from the 5-minute audio clip of the movie "Taken" using pyAudio Analysis, along with the intensity of the original audio clip is shown in Appendix A. These audio features were then used in the GLM to calculate the β-values and then finally the t-maps (Appendix B). From the Appendix B, it can be seen that some of the MFFCs (P8, P9, P11, P13) are properly capturing the auditory perception at each level of consciousness which was observed in the empirical data (Appendix B). MFCCs are frequency-smoothed log-magnitude spectra derived from a sinusoidal-based expansion of the energy spectrum, and demonstrate good representation of speech signals or of human hearing. These coefficients suppress undesirable spectral variation, particularly at higher frequencies, and therefore may be capturing useful acoustic properties related to auditory perception.

The ISC calculated from the simulated data under auditory stimulation using the GIM in the awake, mild sedation, deep sedation, and recovery conditions are displayed in Fig 5. At all four levels of consciousness, at criticality the ISC increases, but at a temperature distant from criticality in the super critical regime (T^*), the ISC of the simulated data closely resembled that of the empirical data. In the awake state, the primary auditory, frontal, and language regions synchronized in the empirical data are again synchronized at T^*. Moreover at T^* there

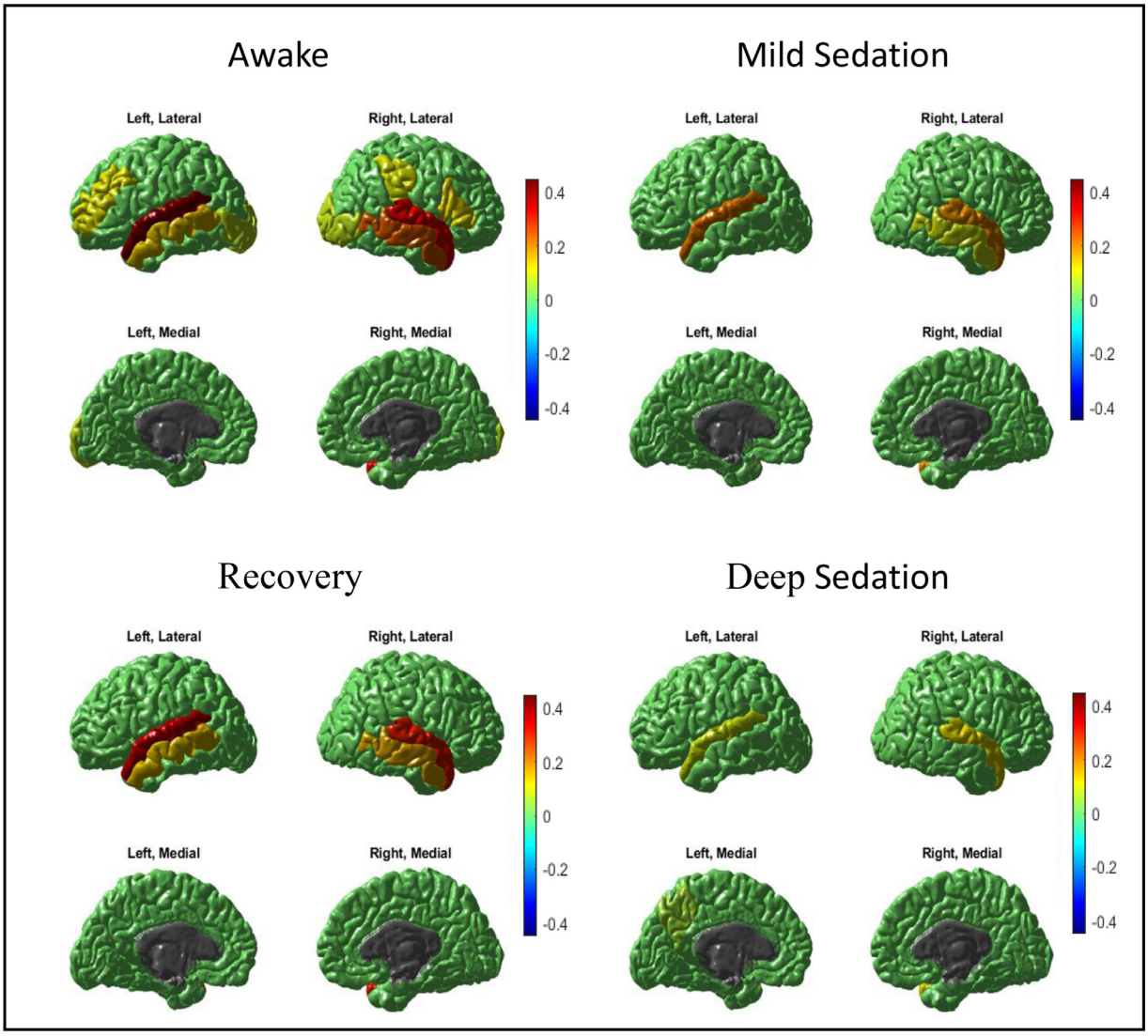

Fig. 1. ISC calculated from the empirical task data at four different levels of consciousness.

were regions that showed synchronization among subjects that was not present in the empirical data. For example, in the simulated data, a paradoxical effect of an increase in synchronization was seen in the motor area of the left hemisphere during mild sedation and a synchronization in the right inferior parietal in deep sedation. Further the correlation between the empirical ISC and simulated ISC maps at T^* for awake, mild sedation, deep sedation and recovery were 0.80, 0.87, 0.61 and 0.83 respectively.

When the GIM was simulated using the permuted $J_{ij,}$ and permuted coupling strengths obtained from the task condition, the temperature at which the best fit between the empirical and simulated ISC (T^*) varied from the original values, i.e. before permuting the J_{ij} and coupling terms. Correlation values calculated between the empirical ISC and simulated ISC at T^* in different conditions is shown in Table 1. It can be seen that, in all conditions, permuting beta values highly reduced the correlation values, while permuting the J_{ij} did not change much the correlation values. These results indicate that although a contribution from the j_{ij} is seen in the ISC, the majority of the contribution comes from the coupling terms between the spins and the external field. Ideally having the scrambled data would have permitted to test the null distribution accurately using different coupling strengths obtained from these data.

4. Discussion

FMRI studies indicate that neuronal responses are more ecologically valid under naturalistic conditions than under conventional laboratory conditions using artificial stimuli (Hasson et al., 2010). Naturalistic paradigms, with the aid of engaging movies or narratives, capture and sustain attention more easily than artificial stimuli or task designs (Naci et al., 2014). Therefore, we investigated the capability of the GIM to fit fMRI data obtained during a naturalistic audio listening task at different levels of consciousness as induced by propofol. The GIM was simulated using the Metropolis Monte Carlo algorithm to obtain equilibrium spin configurations when an external stimulus (i.e. an audio clip) was applied, and the ISC at different temperatures was calculated to find the best fit to the empirical ISC.

Primary auditory, language, and the fronto-parietal regions belonging to the executive control network appear to have strong ISC amongst the participants during the awake and recovery states (Fig. 1, 5). These ISC values diminish during sedation in the empirical and simulated task data. However, in the sedated condition, ISC was present only in primary auditory regions but with smaller values. This is consistent with these regions' roles in auditory perception and processing external information from the environment, such as listening to a story. Previous

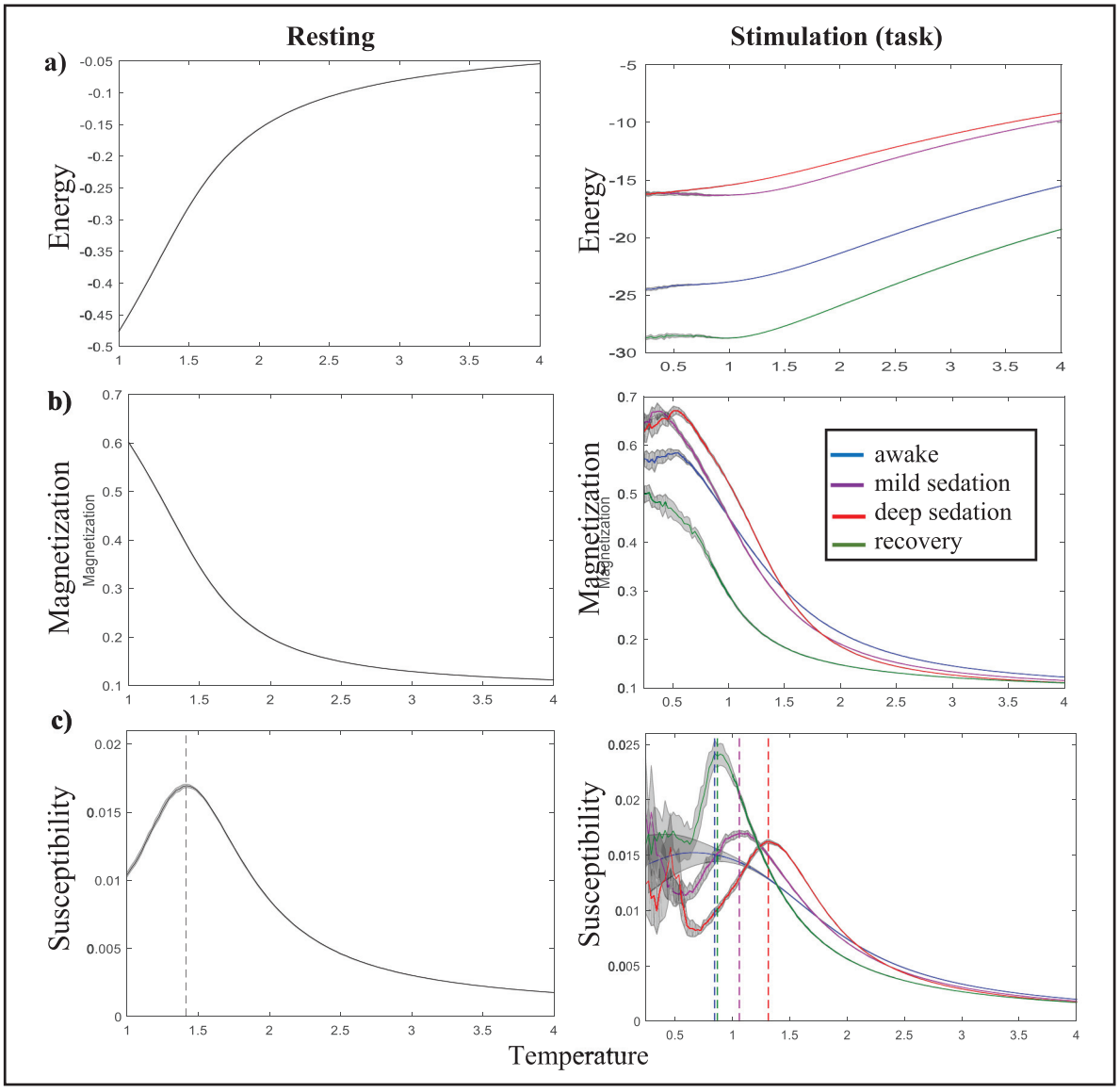

Fig. 2. Thermodynamic properties, a) Magnetization b) Energy c) Susceptibility calculated from the GIM during resting and under stimulation at four different levels of consciousness. The dashed lines represent the critical temperatures.

Table 1
Correlation values calculated between the empirical ISC and simulated ISC at T^* before and after permuting J_{ij} and beta values.

	Awake	Mild Sedation	Deep Sedation	Recovery
J_{ij} and beta	0.782±0.001	0.855±0.002	0.625±0.005	0.825±0.003
Permuted J_{ij}	0.784±0.002	0.865±0.001	0.583±0.005	0.784±0.002
Permuted beta	−0.055±0.003	0.069±0.004	−0.101±0.006	0.113±0.004

* standard deviation was calculated based on the leave one procedure, in which each time one subject's ISC is removed and the mean over the remainder is calculated.

studies have shown decreased activity in the fronto-parietal network of anesthetized brains (Boly et al., 2012; Naci et al., 2018). Loss of information processing in the fronto-parietal regions reveals that complex auditory processing in the higher-order networks—such as the executive control network—is suppressed, but with a reduced amount of processing in the lower-order networks—such as the auditory network—during unconsciousness.

When the brain is auditorily stimulated in the real world, some features of the audio signal negatively couple to certain regions of the brain, while other features positively couple with certain brain regions. This, in turn, moves the system towards a disordered state, shifting the criticality to a lower value as seen in Fig. 2. This may allow the brain to engage only on the necessary regions, and to respond to external stimulation in an effective way. In this case, external stimulation does not behave as a source of order—aligning all the spins in the system in one direction—but appears to behave as a source of disorder.

Under stimulation, critical temperatures during unconsciousness (i.e., deep sedation) moved closer to the spontaneous criticality; and,

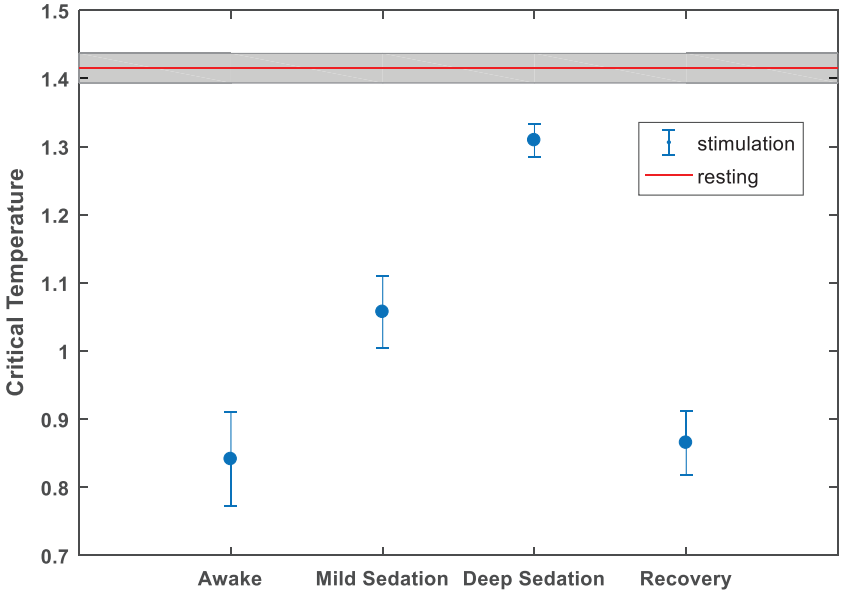

Fig. 3. Critical temperature variation during resting and under stimulation at four different levels of consciousness.

conversely, when participants were conscious, they moved away from spontaneous criticality toward a lower temperature (Fig. 3). When the external stimulus was presented during deep sedation, the system was less affected, and therefore remained closer to the spontaneous criticality, due to the low coupling strengths of the spins with the external stimulus. This is because the *t*-values were small and, therefore, the system resembled spontaneous activity, having a critical value significantly closer to that of the spontaneous situation (Fig. 3). On the other hand, *t*-values were bigger while participants were under stimulation while awake or in recovery, and therefore pushed the system further away from spontaneous criticality, as depicted in Fig. 3. The effect of the audio clip on the awake and recovery states was stronger than in the deep anesthesia state, and the criticality can be considered a measure of the engagement in the story.

Fraimann et al. (Fraiman et al., 2009) had stated that the brain functions at criticality during wakeful rest. However, an ongoing debate concerns whether the brain does indeed function at criticality, and some controversial results were reported by Bédard et al. (Bedard et al., 2006), and Dehghani et al. (Dehghani et al., 2012), using recordings in animals and humans. They had performed avalanche dynamics studies on humans, cats and monkeys using EEG, and reported a lack of power-law scaling, a characteristic of critical behavior, in both awake and sleep states. Our results indicate that when an external stimulus is applied, dynamics show a departure from criticality towards the super-critical state as observed in Fig. 4. Temperature was used as a fitting parameter in order to match conditions in the real brain. Here, the T^* does not only depend on the input J_{ij}, but also depends on how the external stimulus couples with the spins. At rest, Tc is a good approximation and T^* does not move much away from Tc, as there is no ISC. But under stimulation, the ISC constrains the model and T^* moves away from Tc to a higher temperature.

In the Ising model, temperature (T) acts like a thresholding mechanism to maximize the ISC between empirical and simulated data. As T is increased, spins that are mildly coupled with the external field lose their coupling, because the thermal energy provided by the temperature overcomes the interaction between the spins and the external field. This reduces synchronization amongst participants. However, spins that are strongly coupled with the audio clip, for example spins corresponding to auditory regions, still retain their coupling with the field despite the increase in temperature. At Tc, most of the spins are coupled with the external field, producing a high level of synchronization on all spins amongst participants, which is not reflective of the empirical data. But at T^*, only the necessary spins are coupled to the external field, while the other spins are decoupled with the external field. This leads to synchronization in the necessary regions giving the best match with the empirical data. In all four conditions under stimulation, it became necessary to move away from criticality into the super-critical state to find the best match with the empirical task fMRI data (Fig. 4).

An increase in brain activity due to stimulation changes the sensitivity of neuronal inputs and, therefore, the brain may be dynamically moved into different states (Hesse and Gross, 2014) and also may be confined (Ponce-Alvarez et al., 2015) to adapt brain functions of momentary demands. Moreover, some studies have proposed that an external time-varying input may give rise to power-law avalanche distributions, and the larger networks can be restored when the avalanches within the modules are further pushed into the supercritical regime (Dahmen et al., 2019). When the brain is exposed to a significant level of external input, self-tuning mechanisms of the brain might try to regulate the activity down. This will make the system to depart from criticality, in which the internally generated dynamics was optimized (Hesse and Gross, 2014).

The GIM with an external field combined with the novel ISC technique could provide an alternative way to measure the level of awareness of patients with different neuropathological conditions or even in non-responsive patients. In order to assess the awareness of these patients, ISC (which is a measure used in this study to calculate the conscious experience) should be calculated. To attain this goal, the audio clip from the same movie should be played for patients and fMRI data should be acquired. Then GLM should be applied on the fMRI time series by using as predictors the features of the movie (explained in Section 2.10) to obtain the coupling strengths (interaction of the external field with the spins). Afterwards, using disrupted structural connectivities (J_{ij}) of these patients and the extracted coupling strengths, GIM should be simulated to obtain the simulated time series at the temperature T^* which was previously obtained from the healthy subjects' simulations. The ISC map (set of ISC values of each ROI) of each patient can then be obtained by calculating the correlation values between the subject's time series with all the 17 healthy subjects' time series and averaging them. These ISC values will give us an idea of how much the patient's time series is correlated with the healthy subjects time series.

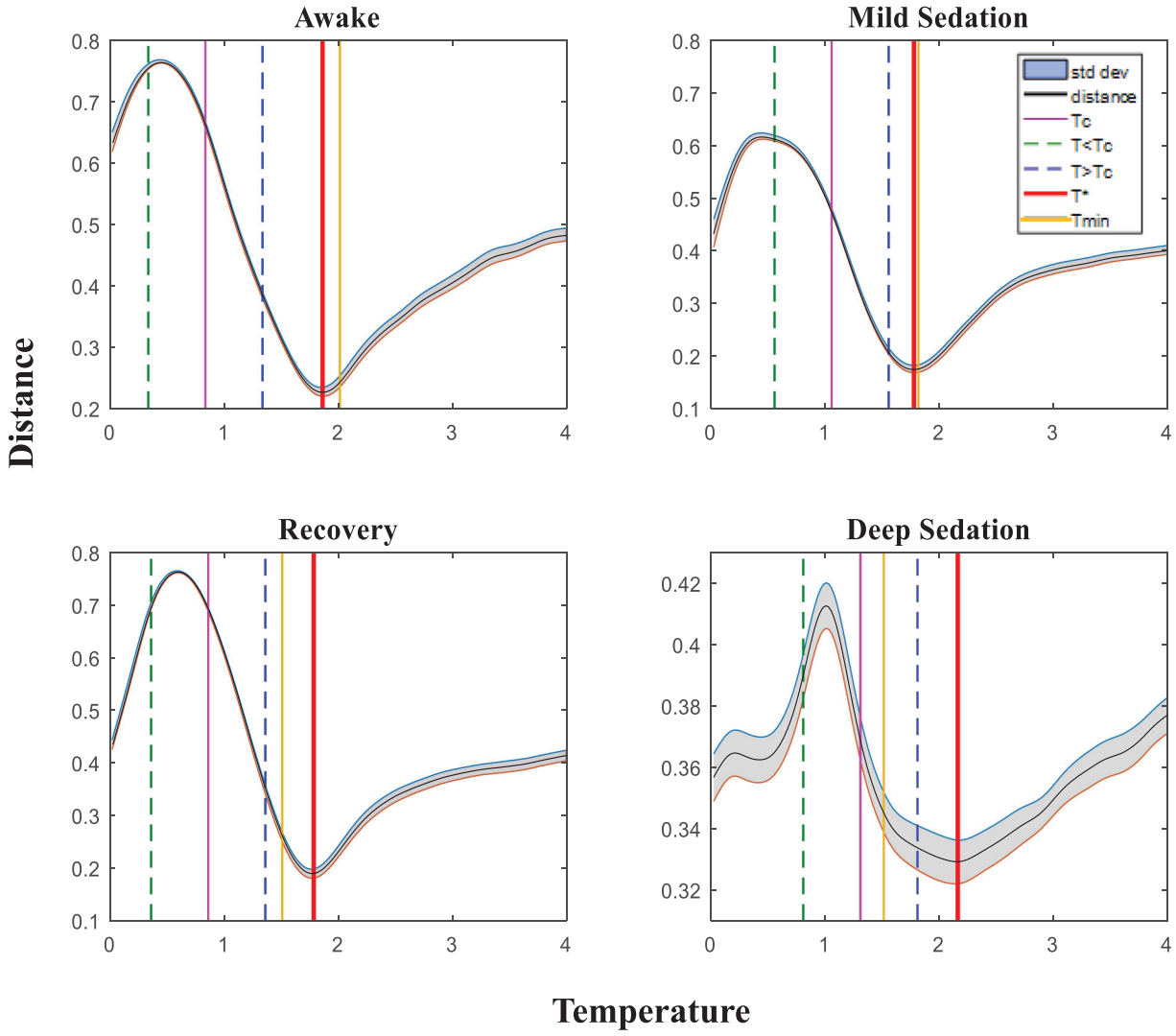

Fig. 4. Distance (calculated using the KS-test) between the empirical and simulated ISC under stimulation, at four different levels of consciousness. The red line represents the temperature that minimized distance between empirical and simulated ISC. Magenta, green dashed, and blue dashed lines represent the critical, sub, and super, critical temperatures, respectively, under stimulation. The orange line (*Tmin*) represents the temperature that minimizes the distance between the empirical and simulated correlation matrices.

Then the statistical significance of the ISC values of the patients can be tested vs the null distribution created from the ISC of healthy subjects. The main advantage of using the GIM is that it can be simulated using the structural connectivity and coupling strengths of these patients which hypothetically can be altered, until a similar ISC, or conscious experience, to the healthy controls is obtained, simulating a possible healing process. The simulations on these patients will depend mainly on the interaction of the patients with the external stimulus while a minor contribution arises from the structural connectivity as well. Coupling strengths can be assumed to be related with the metabolic activity. Astrocytes, are cells in the neuronal system which provide structural and functional support to the neurons and also assist in controlling the metabolic activity, by regulating the blood flow to regions of the brain. Inflammation in these astrocytes tend to inhibit the blood flow, resulting in reduction of metabolic activity. Treating these inflamed astrocytes, might help to re-gain the metabolic activity which in our model will correspond to increase the coupling strengths. Specifically for disorders of consciousness patients, according to our model, it will be more relevant to restore the metabolic activity than the fibers, which in turn will restore the interaction of the external stimulation with the brain regions.

5. Limitations of the study

The main limitation of the study is that we used the fMRI data itself to extract the beta maps. These beta maps were then used to simulate the Ising model to fit the empirical data. Beta maps tell us how the profile of an audio clip will couple to specific regions and which should be universally independent of the audio clip. In the future, using the beta maps extracted from one audio stimulation (audio clip of a movie) to predict the ISC for different audio stimulations would provide better predictive power.

Another limitation of the study is that the model is unable to provide a proper ISC when the external field is only coupled to the primary auditory regions. In the stimulated scenario, more than the structural connectivity, it is the coupling between the stimulus and the brain regions which is more dominant in the model. A very successful model should be able to provide proper ISC, by just coupling the external magnetic field to the primary auditory regions, instead of the full brain. Future research should test the possibility of coupling the external field to primary auditory regions only, while giving different weights to J_{ij}. This would modulate the effective structure for the fiber connectome, taking in to account that the regions of different networks interact differently.

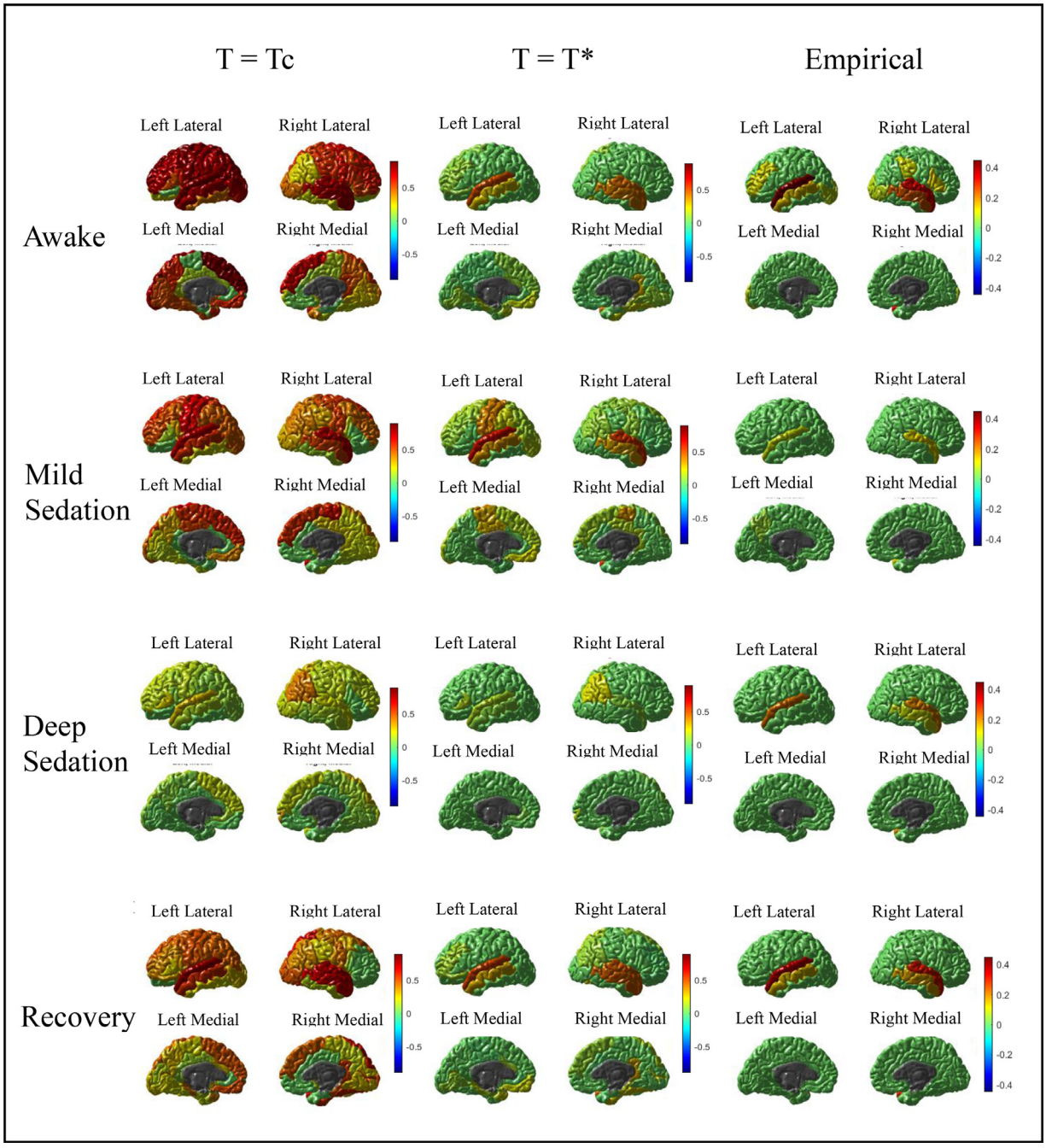

Fig. 5. ISC calculated from the simulated task data at the critical (*Tc*) and at the temperature that minimized the distance between the ISC of the empirical and simulated data (T^*) during awake, mild sedation, deep sedation and recovery.

This would favor the coupling of regions between certain networks with respect to others.

6. Conclusion

The GIM was able to model brain activity under naturalistic stimulation, at different levels of consciousness, using a novel ISC technique. At the temperature T^*, which is in a very super critical state, a similar pattern between the empirical and simulated ISC was observed during stimulation. ISC was not observed in the resting condition at any levels of consciousness, due to the lack of the driving force provided by the external auditory stimulation for synchronization. Distinguishing neural signatures of altered consciousness using the simple GIM may aid in the diagnosis of patients with disorders of consciousness and can provide an indication of how their metabolic activity should be altered in order to regain consciousness.

Declaration of Competing Interest

The authors declare no competing financial interests.

Acknowledgements

This study was funded by the NSERC Discovery grant (05578–2014RGPIN), CERC (215063), CIHR Foundation Fund (167264) and Mitacs Elevate postdoctoral fellowship.

Supplementary materials

Supplementary material associated with this article can be found, in the online version, at doi:10.1016/j.neuroimage.2020.117367.

References

Abreu, et al., 2018. EEG-informed fMRI: a review of data analysis methods. Front Hum Neurosci 12, 29.

Hudetz, 2012. General anesthesia and human brain connectivity. Brain Connect 2 (6), 291–302.

Will & Berg, 2007. Brain wave synchronization and entrainment to periodic acoustic stimuli. In: Neurosci. Lett., 424, pp. 55–60.

Hagihira, 2015. Changes in the electroencephalogram during anaesthesia and their physiological basis. Br J Anaesth 115 (suppl_1), i27–i31.

Tobias & Leder, 2011. Procedural sedation: a review of sedative agents, monitoring, and management of complications. Saudi J Anaesth 5 (4), 395.

Naci, et al., 2014. A common neural code for similar conscious experiences in different individuals. Proceedings of the National Academy of Sciences 111 (39), 14277–14282.

Davis, et al., 2007. Dissociating speech perception and comprehension at reduced levels of awareness. Proceedings of the National Academy of Sciences 104 (41), 16032–16037.

Dueck, et al., 2005. Propofol attenuates responses of the auditory cortex to acoustic stimulation in a dose-dependent manner: a FMRI study. Acta Anaesthesiol Scand 49 (6), 784–791.

Liu, et al., 2012. Propofol disrupts functional interactions between sensory and high-order processing of auditory verbal memory. Hum Brain Mapp 33 (10), 2487–2498.

Schaub & Schultz, 2012. The Ising decoder: reading out the activity of large neural ensembles. J Comput Neurosci 32 (1), 101–118.

Fraiman, et al., 2009. Ising-like dynamics in large-scale functional brain networks. Physical Review E 79 (6), 061922.

Marinazzo, et al., 2014. Information transfer and criticality in the Ising model on the human connectome. PLoS ONE 9 (4), e93616.

Das, et al., 2014. Highlighting the structure-function relationship of the brain with the Ising model and graph theory. Biomed Res Int, 237898.

Stramaglia, et al., 2017. Ising model with conserved magnetization on the human connectome: implications on the relation structure-function in wakefulness and anesthesia. Chaos: An Interdisciplinary Journal of Nonlinear Science 27 (4), 047407.

Deco, et al., 2012. How anatomy shapes dynamics: a semianalytical study of the brain at rest by a simple spin model. Front Comput Neurosci 6, 68.

Abeyasinghe, et al., 2018. Role of dimensionality in predicting the spontaneous behavior of the brain Using the classical Ising model and the Ising model implemented on a structural connectome. Brain Connect 8 (7), 444–455.

Naci, et al., 2017. Detecting and interpreting conscious experiences in behaviorally non-responsive patients. Neuroimage 145, 304–313.

Marsh, et al., 1991. Pharmacokinetic model driven infusion of propofol in children. BJA: British J. Anaesthesia 67 (1), 41–48.

Nimmo, et al., 2019. Guidelines for the safe practice of total intravenous anaesthesia (TIVA Joint Guidelines from the Association of Anaesthetists and the Society for Intravenous Anaesthesia. Anaesthesia 74 (2), 211–224.

Sukumar, et al., 2018. Effect site concentration of propofol at induction and recovery of anaesthesia-A correlative dose-response study. Indian journal of anaesthesia 62 (4), 263.

Hagmann, et al., 2008. Mapping the structural core of human cerebral cortex. PLoS Biol. 6 (7), e159.

Giannakopoulos, 2015. pyaudioanalysis: an open-source python library for audio signal analysis. PLoS ONE 10 (12), e0144610.

Hasson, et al., 2004. Intersubject synchronization of cortical activity during natural vision. Science 303 (5664), 1634–1640.

Pajula, et al., 2012. Inter-subject correlation in fMRI: method validation against stimulus–model based analysis. PLoS ONE 7 (8), e41196.

Kauppi, et al., 2010. Inter-subject correlation of brain hemodynamic responses during watching a movie: localization in space and frequency. Front Neuroinform 4, 5.

McDonald, 2009. In: Handbook of Biological Statistics, 2. Sparky House Publishing, Baltimore, MD, pp. 6–59.

Boveroux, et al., 2010. Breakdown of within-and between-network resting state fMRI connectivity during propofol-induced loss of consciousness. Anesthesiology 113 (5), 1038–1053.

Jordan, et al., 2013. Simultaneous electroencephalographic and functional magnetic resonance imaging indicate impaired cortical top–down processing in association with anesthetic-induced unconsciousness. The J. American Society of Anesthesiologists 119 (5), 1031–1042.

Naci, et al., 2018. Functional diversity of brain networks supports consciousness and verbal intelligence. Sci Rep 8 (1), 13259.

Hasson, et al., 2010. Reliability of cortical activity during natural stimulation. Trends Cogn. Sci. (Regul. Ed.) 14 (1), 40–48.

Boly, et al., 2012. Connectivity changes underlying spectral EEG changes during propofol-induced loss of consciousness. Journal of Neuroscience 32 (20), 7082–7090.

Bedard, et al., 2006. Does the 1/f frequency scaling of brain signals reflect self-organized critical states? Phys. Rev. Lett. 97 (11), 118102.

Dehghani, et al., 2012. Avalanche analysis from multielectrode ensemble recordings in cat, monkey, and human cerebral cortex during wakefulness and sleep. Front Physiol 3, 302.

Hesse, J., Gross, T., 2014. Self-organized criticality as a fundamental property of neural systems. Front Syst Neurosci 8, 166.

Ponce-Alvarez, et al., 2015. Task-driven activity reduces the cortical activity space of the brain: experiment and whole-brain modeling. PLoS Comput. Biol. 11 (8), e1004445.

Dahmen, et al., 2019. Second type of criticality in the brain uncovers rich multiple-neuron dynamics. Proceedings of the National Academy of Sciences 116 (26), 13051–13060.